Permanent excimer superstructures by supramolecular networking of metal quantum clusters

Beatriz Santiago-Gonzalez[1],[*], Angelo Monguzzi[1],[*],[†], Jon Mikel Azpiroz[2],[3], Mirko Prato[4], Silvia Erratico[5], Marcello Campione[6], Roberto Lorenzi[1], Jacopo Pedrini[1], Carlo Santambrogio[7], Yvan Torrente[5], Filippo De Angelis[2],[4], Francesco Meinardi[1],[†], Sergio Brovelli[1],[†]

1Dipartimento di Scienza dei Materiali, Università degli Studi di Milano-Bicocca, Via R. Cozzi 55, 20125 Milano, Italy.
2Computational Laboratory for Hybrid and Organic Photovoltaics, National Research Council–Institute of Molecular Science and Technologies (CNR-ISTM), Via Elce diSotto 8, 06123 Perugia, Italy.
3Kimika Fakultatea, Euskal Herriko Unibertsitatea (UPV/EHU), and Donostia International Physics Center, 20080 Donostia, Euskadi, Spain.
4Istituto Italiano di Tecnologia, Via Morego 30, 16163Genova, Italy.
5Dipartimento di Fisiopatologia Medico-Chirurgica e dei Trapianti, Università degli Studi di Milano, Fondazione IRCCS (Istituto di Ricovero e Cura a Carattere Scientifico) Cá Granda Ospedale Maggiore Policlinico, Centro Dino Ferrari, Via Francesco Sforza 35, 20122 Milano, Italy.
6Dipartimento di Scienze dell'Ambiente e del Territorio e di Scienze della Terra, Università degli Studi Milano-Bicocca, Piazza della Scienza, 20125 Milano, Italy.
7Dipartimento di Biotecnologie e Bioscienze, Università degli Studi Milano-Bicocca, Piazza della Scienza, 2 20126 Milano, Italy.
**These authors contributed equally to this work.*
†Corresponding author. Email: angelo.monguzzi@mater.unimib.it (A.M.);meinardi@mater.unimib.it (F.M.); sergio.brovelli@unimib.it (S.B.)

Abstract

Excimers are evanescent quasi-particles that typically form during collisional intermolecular interactions and exist exclusively for their excited-state lifetime. We exploited the distinctive structure of metal quantum clusters to fabricate permanent excimer-like colloidal superstructures made of ground-state noninteracting gold cores, held together by a network of hydrogen bonds between their capping ligands. This previously unknown aggregation state of matter, studied through spectroscopic experiments and ab initio calculations, conveys the photophysics of excimers into stable nanoparticles, which overcome the intrinsic limitation of excimers in single-particle applications—that is, their nearly zero formation probability in ultra-diluted solutions. In vitro experiments demonstrate the suitability of the superstructures as nonresonant intracellular probes and further reveal their ability to scavenge reactive oxygen species, which enhances their potential as anticytotoxic agents for biomedical applications.

Metal quantum clusters are functional nanoscale materials with potential for use in sensing (***1***), bio imaging (***2***), optoelectronics (***3***), and nanomedicine (***4***). With "magic" sizes dictated by the valence of the metal constituents (***5***) and dimensions approaching the Fermi wavelength of the electron, these few-atom structures bridge the gap between atoms and colloidal nanoparticles. As a result, metal quantum clusters combine a molecule-like electronic structure with quantum confinement effects that confer them with size- and shape-tunable optical properties, ultralarge surface-to-volume ratios, and unmatched flexibility for tailoring their physical properties through surface functionalization. Specifically, ligand-to-metal electron transfer (LM-ET) in metal quantum clusters with electron-rich capping agents (***6***–***8***) leads to strongly Stokes-shifted emission, which is beneficial for photon management (***9***) and bio imaging (***1***) applications. On the other hand, suppression of LM-ET results in intrinsic luminescence, with energy determined by the quantum mechanical combination of single-atom electronic orbitals (***10***, ***11***). Fundamentally, the key common feature of "intrinsic emitting" metal quantum clusters is their capping with bulky molecules (***12***–***15***) or their encapsulation in supramolecular vesicles (***14***, ***16***, ***17***), imposing large distances between the metal cores. The use of short ligands, even in the absence of LM-ET, has led instead to a variety of optical behaviors (***18***–***21***). This points to a role of intercluster interactions in the photophysics of metal quantum clusters and suggests a supramolecular strategy for tuning their optical

properties through controlled formation of aggregate species, similarly to what is achieved with organic chromophores.

In molecular physics, aggregate species are typically divided into two main categories based on the type of interaction that leads to their formation: Molecular dimers arise from ground-state interactions between individual moieties (monomers) (***22***), whereas excimers are evanescent quasi-particles existing exclusively in the excited state and formed through the aggregation of an excited monomer and a ground-state monomer. When excimers return to the ground state, their constituent monomers dissociate (***22***). As a result, dimers are capable of ground-state absorption, whereas excimers exhibit the absorption spectrum of the monomers and long-lived Stokes-shifted emission from lower-lying intermolecular states. Molecular excimers are typically formed through collisional interactions between monomers in concentrated solutions, and their formation probability drops to zero upon dilution (***23***). The excimer motif is, therefore, intrinsically prevented from being used for the fabrication of stable, self-standing emitters for single-particle applications.

In this work, we overcame this limitation by demonstrating a previously unknown aggregation state of matter that conveys the photophysics of excimers into individual particles that can find application as nonresonant emitters in cellular imaging and integrated photonic nanotechnologies. Specifically, we used Au_n (gold quantum clusters consisting of *n* atoms) as building blocks for fabricating permanent excimer-

like colloidal superstructures (Au-pXs) held together by a network of hydrogen bonds between their capping ligands. As a result of repulsive forces between the metal cores, in the ground state, the networked Au_n behave as independent chromophores, whereas on photoexcitation, they form bimolecular excimers with largely Stokes-shifted emission (~1 eV). In contrast, encapsulation of Au_n in bulky vesicles hinders the excimeric interaction, resulting in the photophysics of isolated clusters. Last, we used Au-pXs for in vitro imaging of fibroblast cells. Our data reveal the high biocompatibility of Au-pXs and their ability to scavenge reactive oxygen species (ROS) responsible for premature cellular death, thereby further enhancing their potential for biomedical applications.

Figure 1 depicts the synthetic routes for obtaining isolated and networked clusters. Both samples were produced by etching of gold nanoparticles (fig. S1) with 11-mercaptoundecanoic acid (MUA) ligands that bond to the gold atoms through their thiol end group while exposing their carboxylic functionality (***24***). Critical to the fabrication of isolated clusters is the suppression of the H-bond capability of the ligands; this can be achieved by adding tetraoctylammonium bromide (TOABr), which leads to the formation of Au_n encapsulated in $(MUA^-)(TOA^+)$ vesicles (hereafter referred to as encapsulated clusters) (***11***). In the absence of the vesicles, the hydrogen bonding between the carboxylic functionalities of MUA^- leads to the formation of Au-pXs. The size of the synthesized clusters and the composition of the ligand shell were investigated by means of electrospray ionization mass spectrometry and x-ray

photoelectron spectroscopy, which indicated that both routes produce Au_8 clusters capped by four MUA units (figs. S2 and S3 and tables S1 and S2).

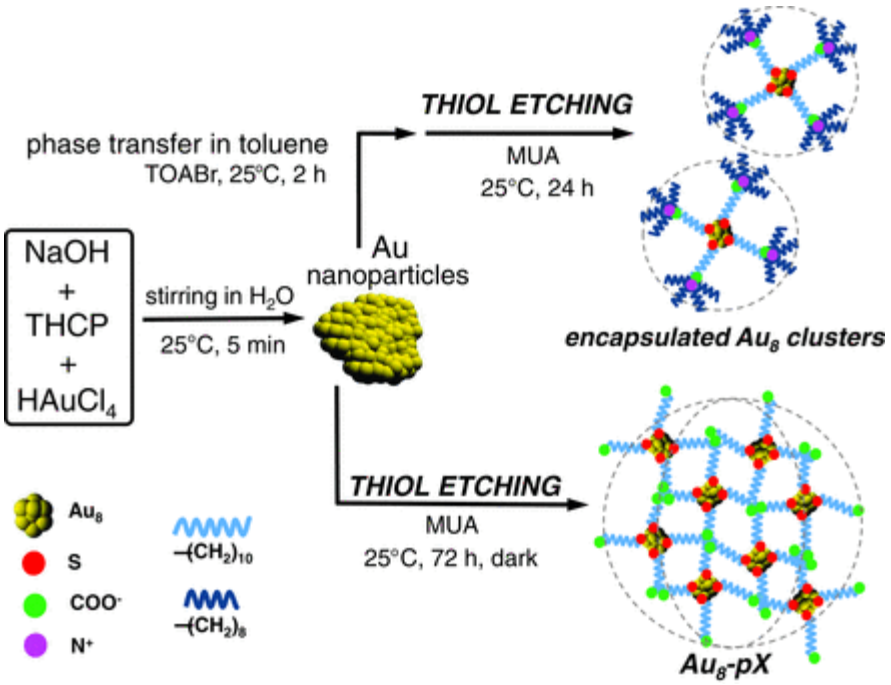

Fig. 1 Synthesis of encapsulated and networked gold quantum clusters.

The diagram illustrates the protocols for synthesizing encapsulated Au_8 and networked superstructures (Au-pXs) by thiol-induced etching of gold nanoparticles. Au-pXs are obtained by networking of MUA-capped clusters. Phase transfer using TOABr in toluene leads instead to isolated clusters. THCP, tetrakis(hydroxymethyl)phosphonium chloride; h, hours.

The optical absorption, photoluminescence (PL), and PL excitation (PLE) spectra of the synthesized materials are shown in **Fig. 2A**, together with the respective PL decay traces (**Fig. 2, B and C**). Both samples show narrow spectral features indicating monodispersity of the cluster size. The optical absorption and PLE spectra peak at 3.22

eV, corresponding to the ground-state absorption energy predicted by the jellium model for Au_8 (***25***). The essentially identical absorption profiles and cross sections for encapsulated and networked clusters confirm that the size of the gold cores is unaffected by the phase transfer with TOABr and that, in both cases, the Au_8 cores are noninteracting in the ground state.

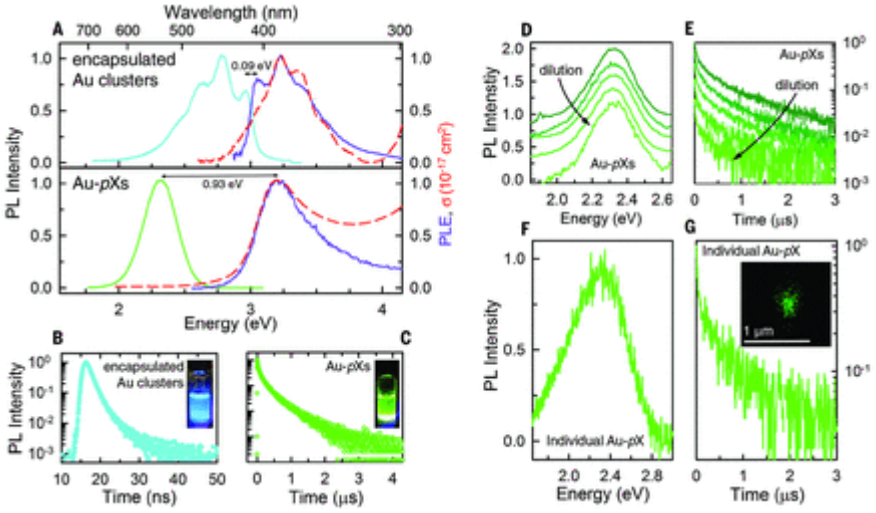

Fig. 2 Optical properties of encapsulated and networked gold quantum clusters.

*(**A**) Absorption cross section (σ, dashed red lines), PL (blue and green lines for encapsulated Au and Au-pXs, respectively), and PLE (purple lines) spectra recorded at the maximum of emission. The Stokes shift is indicated by the black arrows. (**B**) Time-resolved PL measurements of encapsulated clusters and (**C**) Au-pXs. The insets are photographs of the two systems under ultraviolet illumination. (**D**) Normalized PL spectra and (**E**) PL decay profiles of Au-pXs in water at increasing dilution (as indicated by the arrow): from dark to light green, 740, 148, 74, 7.4, and 0.74 μM. (**F**) PL spectrum and (**G**) respective decay curve of an individual Au-pX on glass. The inset*

is a confocal fluorescence image of the same particle. All measurements were performed using 3.25 eV excitation.

Despite such similarity, encapsulated clusters and Au-pXs exhibit striking differences between their PL spectra and decay dynamics. Encapsulated systems show blue PL at ~2.75 eV, mirroring their absorption profile with distinct vibronic replica with an energy separation of ~175 meV, due to coupling with the C-H vibrations of the ligands. The PL quantum yield is Φ_{PL} = 12 ± 2%. The total PL lifetime of the encapsulated clusters is τ_{tot}^{enc} = 1.6 ns, which yields a radiative decay time $\tau_{rad}^{enc} = \tau_{tot}^{enc}/\Phi_{PL}$ = 13.3 ns, in good agreement with the radiative lifetime obtained through the Strickler-Berg analysis (12.0 ns) and with dendrimer-templated Au_8 [18.0 ns; fig. S4 and (***25***)]. This confirms the encapsulation of individual clusters into (MUA^-)(TOA^+) vesicles and the absence of LM-ET. In contrast, the PL spectrum of Au-pXs is featureless and peaks at ~2.36 eV (Φ_{PL} = 4.5 ± 0.8%), resulting in a Stokes shift of ~0.93 eV. The decay dynamics extend to the microsecond time regime, with average lifetime τ_{tot}^{Au-pX} = 114 ns. In this case, the radiative lifetime extracted from the decay trace, τ_{rad}^{Au-pX} = 2.5 µs, is over 200 times as long as the radiative lifetime τ_{rad}^{Au-pX} = 11.4 ns obtained through the Strickler-Berg analysis. This indicates that the long-lived emission of Au-pXs does not arise from the absorbing state. Both samples feature MUA ligands, which excludes LM-ET as a possible origin of the Stokes-shifted PL of Au-pXs. The PL decay trace in **Fig. 2C** shows no measurable rise time, indicating that such emission does not arise from a subpopulation of larger clusters excited through energy transfer from the dominant

fraction of Au_8 that is responsible for the absorption profile (supplementary materials).

The photophysical phenomenology can be comprehensively described by the behavior of a molecular excimer (***22***). Our metal-cluster excimers present a fundamental difference with respect to conventional excimers, that is, their formation is independent of the monomer density. This is confirmed by data in **Fig. 2, D and E**, showing that both the PL spectra and the decay dynamics of water solutions of Au-pXs are unaffected by increasing the dilution by over four orders of magnitude. This behavior is unexpected because, in contrast to ground-state aggregation, whose reaction equilibrium can be shifted in favor of dimerization regardless of the monomer concentration, the formation of excimers is a collisional bimolecular process that occurs exclusively within the monomer excited-state lifetime. Excimer formation is, therefore, strongly concentration-dependent, with probability dropping to zero at low monomer densities (***22***). As a result, with increasing dilution, the emission profile and decay dynamics of molecular excimers evolve toward the behavior of the isolated monomers (***22***). The invariance of the spectral and dynamical properties of Au-pXs with increasing dilution indicates that the Au_8 are in close proximity to each other in concentration regimes where conventional chromophores behave as isolated monomers. Despite such a coalescence state, ground-state interaction is hindered, and optical excitation is required for the formation of a bound system in which the excited-state wavefunction is delocalized over two or more

Au_8 cores. To assess the persistence of Au-pXs in “infinite” dilution conditions, we performed spectroscopic measurements of individual superstructures. Single-particle data shown in **Fig. 2, F and G**, reveal identical PL spectra and decay dynamics to those of the aqueous solutions, which unambiguously confirms that each Au-pX behaves as a permanent excimer at the single-particle level.

Transmission electron microscopy images enabled us to visualize the Au-pXs (fig. S5), which appear as isolated spheroid structures with a radius of ~4 to 5 nm, probably resulting from the coalescence of several Au_8 clusters. To investigate the cohesive forces responsible for intercluster networking, we conducted Fourier transform infrared transmission (FT-IR) experiments on encapsulated Au_8 and Au-pXs. The data shown in fig. S6 indicate that the carboxylic hydrogen atoms are retained in Au-pXs, leading to the formation of hydrogen bonds between the carboxylic terminals of the MUA ligands. PL experiments conducted while titrating the Au-pX solution with NaOH or HCl (fig. S7) indicate that hydrogen networking between the ligands introduces strong cohesive forces that preserve the supramolecular architecture in harsh pH conditions.

To gain deeper insight into the physical mechanism underpinning the photophysics of Au-pXs, we performed ground- and excited-state density functional theory (DFT) and time-dependent DFT (TD-DFT) calculations. Building on the experimental evidence and preliminary screening calculations (figs. S8 to S10), we selected a star-shaped

$[Au_8(MUA)_4]^{4-}$ cluster with C2 alkyl chains as a starting model monomer (**1** in **Fig. 3A**). Ground-state geometry optimizations reveal a strong propensity to form carboxylic acid dimers (**2.1**), with a formation energy exceeding 1 eV even after correcting for the translational and rotational entropic losses. A secondary configuration is characterized by strong reconstruction of the two interacting Au_8 cores (**2.2**). Given its high stability, **2.1** is probably the species that dominates the solution equilibrium (**Fig. 3B**). The TD-DFT–calculated absorption profiles are shown in **Fig. 3C**. Notably, **2.1** shows essentially the same absorption maximum and spectral shape as the monomer, in excellent agreement with the measured absorption spectra and with the jellium model. The energy stabilization of **2.1** (**Fig. 3B**) is thus due to the ligand interactions, with negligible electronic perturbation of the Au_8 cores. A broader and red-shifted spectrum calculated for **2.2**, reflecting the perturbation of the electronic structure caused by formation of the reconstructed Au_{8+8} aggregate. Although the high stability of **2.1** correlates with the lack of free carboxylic groups observed by means of FT-IR (fig. S6), it cannot explain the excimeric behavior, which must relate to a species that is stable exclusively in the excited state. Structure **2.2** cannot be such a species, because it shows free carboxylic groups and its ground state is lower in energy than that of structure **1** (**Fig. 3A**). Furthermore, when capped with C11 chains, structure **2.2** is too high in energy to be favorably formed in the excited state (fig. S10). We have thus considered two interacting aggregates, leading to larger structures involving four Au_8 cores, **4.1** and **4.2** in **Fig. 3A**. **4.1** has two almost intact

staggered cores, whereas **4.2** shows a reconstruction of the two interacting cores, similar to **2.2**. Structure **4.1** is considerably less energetically stable than twice the energy of **2.1** (including entropic losses), whereas the formation of **4.2** is ~0.5 eV disfavored in the ground state but is favored by ~0.2 eV in the bright excited state (**Fig. 3B**). Neglecting further excited-state relaxation, we calculate that **4.2**should emit at 2.3 eV (2.0 eV) in the bright (lowest) excited state, and both of these values are consistent with the experimental data. A plausible excimer structure seems therefore related to a reconstructed Au_{8+8} metal core.

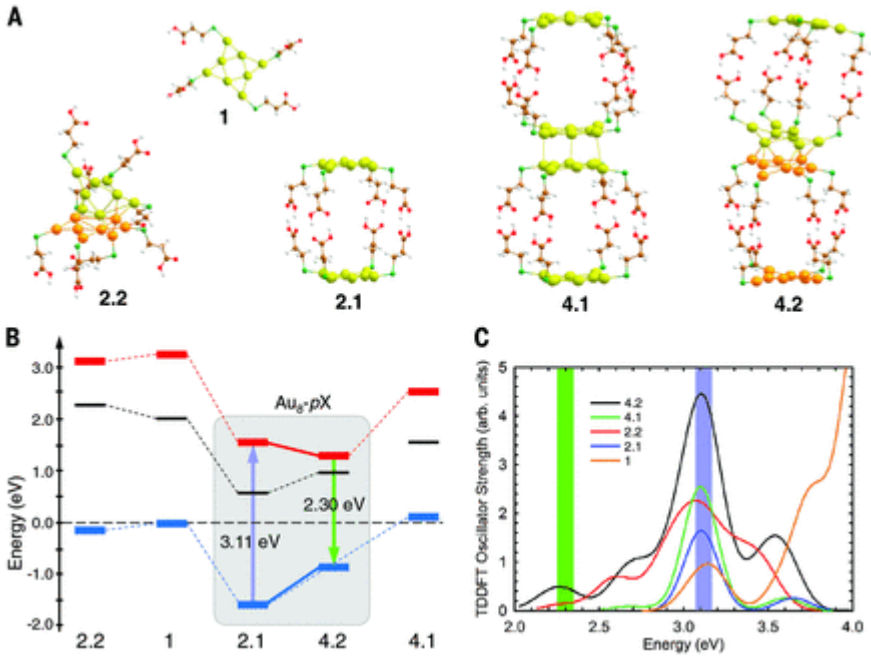

Fig. 3 DFT and TD-DFT calculations. *(**A**) Optimized molecular structures of the $[Au_8(MUA)_4]^{4-}$ model monomer with C2 alkyl chains (**1**), of a dimer and tetramers linked by hydrogen bonds between their carboxylic end groups (**2.1**, **4.1**, and**4.2**), and of a dimer interacting only through the Au_8 cores (**2.2**). Au, yellow; S, green; O, red; C, brown; H, white. For **2.2** and **4.2**, yellow and orange are used for gold atoms*

*belonging to different starting monomers. (**B**) Energy diagrams for the ground state (blue), dark excited state (black), and bright excited state (red) of the modeled species (listed on the x axis). An excimer formation from **2.1** to **4.2** is highlighted in the shaded area. (**C**) Absorption spectra of the various structures, calculated by TD-DFT/CAM-B3LYP (a hybrid exchange–correlation functional). The vertical bars represent the experimental absorption (purple) and emission (green) energies, corresponding to the colored arrows in (B). arb., arbitrary.*

To validate the applicative potential of Au-pXs for cellular imaging and to assess their stability in biological media, we performed in vitro experiments on 3T3 fibroblast cells. Shown in **Fig. 4, A and B**, are bright-field and fluorescence images of cells stained with Au-pXs and with DAPI (4',6-diamidino-2-phenylindole), and PKH-26 dyes, which respectively mark the nucleus and the cellular membrane. Because Au-pXs are not functionalized with target-specific ligands, they disperse in the cytoplasm. Fluorescence microscopy of cells with unstained nuclei confirmed the internalization of Au-pXs, producing excellent-quality images when using the green and red detection channels for Au-pXs and PKH-26, respectively (**Fig. 4, C and D**). In the absence of Au-pXs, only the red emission of PKH-26 was observed (**Fig. 4, E and F**).

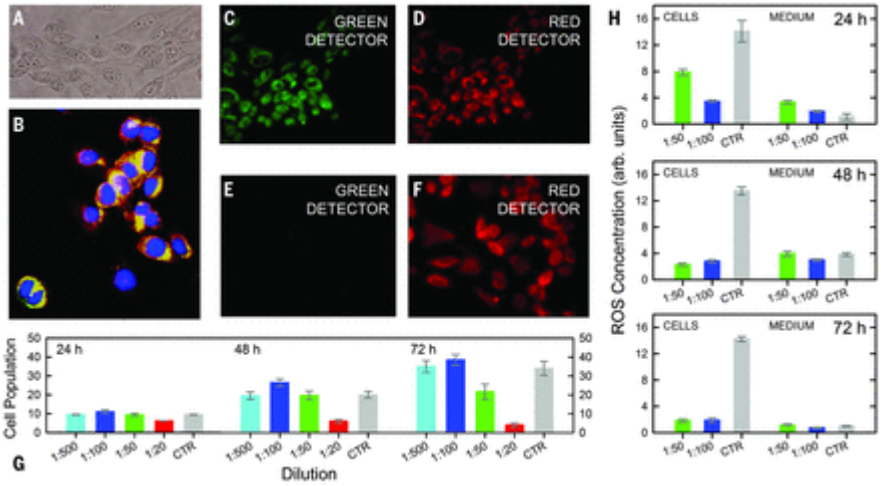

Fig. 4 Cellular imaging and radical oxygen scavenging using Au-pXs.

*(**A**) Bright-field image of 3T3 stem cells on glass. (**B**) Fluorescence image of fixed cells stained with DAPI (blue), Au-pXs (green), and PKH-26 (red). (**C** and **D**) Confocal fluorescence images of 3T3 cells stained with Au-pXs and PKH-26 and (**E** and **F**) only PKH-26 for direct comparison (excitation at 3.25 eV for all images). (**G**) MTT test on 3T3 cells stained with Au-pXs at increasing concentrations (from 1:500 to 1:20 dilution of the 740-μM mother solution) at three time points during cell proliferation. CTR, control. (**H**) ROS test on 3T3 cells stained with Au-pXs at 1:500 and 1:100 dilution of the mother solution. Error bars are the standard deviation of the mean values calculated for five independent experiments.*

To evaluate the cell viability and potential effects of Au-pXs on cellular biology, we performed the 3-(4,5-dimethylthiazol-2-yl)-2,5-diphenyltetrazolium bromide (MTT) assay and monitored the concentration of ROS over time. ROS are typically formed as byproducts of the oxygen metabolism. They play important roles in cell signaling and

homeostasis (***26***), but they can become cytotoxic at high concentrations, causing damage to cell structures and possibly leading to cell death or apoptosis (***26***, ***27***). **Figure 4G** shows the results of the MTT assay on cells stained with increasing concentrations of Au-pXs, showing that cell proliferation is unaffected by Au-pXs, except at the highest concentration. This staining level is orders of magnitude higher than that of standard biomarkers such as PKH-26 (~1 μM). The data shown in **Fig. 4H** reveal the beneficial effect of Au-pXs on the metabolisms of 3T3 cells, which, regardless of the cluster content, show a markedly lower ROS level relative to unstained cells. Furthermore, Au-pXs behave as ROS scavengers, reducing the ROS concentration by over a factor of 4 in cells incubated for 72 hours with the 1:50-diluted Au-pX solution. This effect was also observed in control experiments using a saturated aqueous solution of H_2O_2 (fig. S11). The ROS scavenging behavior of Au-pXs could be linked to the reported catalytic effect of Au_n on chemical and photochemical reactions involving oxygen (***28***, ***29***), and it suggests potential applications for Au-pXs as fluorescent probes with therapeutic capability.

By using the capping ligands to control intermolecular interactions between metal quantum clusters, we have demonstrated a previously unknown aggregation state of matter that conveys the photophysics of excimers into stable self-standing particles. This type of excited-state intermolecular aggregation adds a degree of freedom for designing colloidal metal nanostructures with electronic properties that are controllable at the supramolecular level, a property which, up until now, was

exclusive to organic-based architectures. Bio imaging experiments performed on living cells highlight the biocompatibility of our structures and their ability to scavenge cytotoxic agents. The approach that we have demonstrated with Au clusters is not size- or composition-specific and could be applied to different metals or alloys, allowing the realization of permanent excimeric superstructures with predesigned optical and electronic properties.

Acknowledgments: This work is dedicated to the loving memory of Jon Mikel Azpiroz, colleague and friend. B.S.-G., F.M., R.L., and S.B. acknowledge support from the Cariplo Foundation (grants 2012-0844 and 2012-0920). S.B. thanks the European Commission's Seventh Framework Programme (FP7) for financial support under grant agreement no. 324603 (EDONHIST project). The data presented in this report are available upon request to S.B.

Reference:

1. L. Zhang, E. Wang,Nano Today 9,132–157 (2014).
2. C.-A. J. Linet al.,ACS Nano 3, 395–401 (2009).
3. W. Qin, J. Lohrman, S. Ren, Angew. Chem. Int. Ed. 53,7316–7319 (2014).
4. L. Shang, S. Dong, G. U. Nienhaus,Nano Today 6,401–418 (2011).
5. A. Fernando, K. L. D. M. Weerawardene, N. V. Karimova,C. M. Aikens,Chem. Rev. 115, 6112–6216 (2015).

6. F. Aldeek, M. A. H. Muhammed, G. Palui, N. Zhan, H. Mattoussi, ACS Nano, 2509–2521 (2013).

7. J. Chen, Q.-F. Zhang, T. A. Bonaccorso, P. G. Williard,L.-S. Wang, J. Am. Chem. Soc. 136,92–95 (2014).

8. K. G. Stamplecoskie, P. V. Kamat,J. Am. Chem. Soc. 136,11093–11099 (2014).

9. F. Meinardiet al.,Nat. Nanotechnol. 10,878–885 (2015).

10. R. Jin, S. Egusa, N. F. Scherer, J. Am. Chem. Soc. 126,9900–9901 (2004).

11. Z.Wang,W.Cai,J.Sui, ChemPhysChem 10,2012–2015 (2009).

12. B. Santiago Gonzálezet al., Nano Lett. 10, 4217–4221 (2010).

13. X. Huanget al.,J. Phys. Chem. C 116, 448–455 (2012).

14. W.Guo,J.Yuan,E.Wang, Chem. Commun. 48,3076–3078 (2012).

15. T. A. C. Kennedy, J. L. MacLean, J. Liu,Chem. Commun. 48,6845–6847(2012).

16. K. Pyoet al., J. Am. Chem. Soc. 137,8244–8250 (2015).

17. H. Duan, S. Nie, J. Am. Chem. Soc. 129, 2412–2413 (2007).

18. C.-C. Huang, Z. Yang, K.-H. Lee, H.-T. Chang,Angew. Chem.Int. Ed. 46, 6824–6828 (2007).

19. X. Yang, M. Shi, R. Zhou, X. Chen, H. Chen, Nanoscale 3,2596–2601 (2011).

20. V. Venkatesh, A. Shukla, S. Sivakumar, S. Verma, ACS Appl.Mater. Interfaces 6, 2185–2191 (2014).

21. J. Meiet al.,Adv. Mater. 26, 5429–5479 (2014).

22. J. B. Birks,Photophysics of Aromatic Molecules (Wiley-Interscience, 1970).

23. J. R. Lakowicz,Principles of Fluorescence Spectroscopy (Springer, 2010).

24. J. Huanget al., Angew. Chem. Int. Ed. 50,401–404 (2011).

25. J. Zheng, C. Zhang, R. M. Dickson, Phys.Rev.Lett. 93, 077402 (2004).

26. J. M. Matés, J. A. Segura, F. J. Alonso, J. Márquez,Arch.Toxicol. 82, 273–299 (2008).

27. W. Fiers, R. Beyaert, W. Declercq, P. Vandenabeele, Oncogene 18, 7719–7730 (1999).

28. Y. Gao, N. Shao, Y. Pei, Z. Chen, X. C. Zeng, ACS Nano 5,7818–7829 (2011).

29. Z. Jianget al., J. Phys. C 111, 12434–12439 (2007).